Available online at www.sciencedirect.com
ScienceDirect
International Journal of Heat and Mass Transfer 51 (2008) 3896–3905
International Journal of HEAT and MASS TRANSFER
www.elsevier.com/locate/ijhmt

Modeling liquid jet breakup in high speed cross-flow with finite-conductivity evaporation

M.S. Balasubramanyam, C.P. Chen *

Department of Chemical and Materials Engineering, University of Alabama in Huntsville, Huntsville, AL 35899, United States

Received 23 July 2007; received in revised form 15 November 2007
Available online 3 March 2008

Abstract

Numerical study of liquid atomization/spray process in a high speed cross-flow is described in this paper. Due to the strong aero-thermal dynamics/spray interaction, droplet evaporation process plays an important role even for non-chemical reacting cold-flow systems. Further to the development of the finite-conductivity spray evaporation model, an improved drag coefficient correlation which would capture the spray phenomenon more accurately specifically for application to high speed flow applications was also incorporated. Numerical results indicated that jet penetration increased rapidly in the vicinity of the injector exit and then gradually increased due to increase in the drag of the air stream. The predicted results were reasonably comparable to measured data and showed more accurate comparisons to that of the infinite-conductivity model.

Keywords: Spray evaporation; Turbulent atomization; Jet in high speed cross-flow

1. Introduction

The study of the liquid atomization process in a high speed cross-flow has become an important area of research in air-breathing combustion processes, such as Scramjet engines. Their performance depends strongly on the liquid atomization and mixing processes between the liquid fuel spray and the freestream air. The fuel breakup process in a cross-flow involves the effects of liquid column/drop deformation, displacement, and multiple-mode breakups and subsequent fuel droplet dispersion. The dynamics and interaction between the spray jet and cross-flow offer the potential of adjusting jet penetration and droplet dispersion to provide optimal performance across the entire duty cycle of the engine.

The spray quality produced from jet atomization by a cross-flow can be characterized by liquid mass and droplet distributions of the spray. Mass distributions of the spray give an indication of the dispersement and the spatial extent of the liquid in the flow. Knowledge of the droplet velocity profiles aids in assessing fuel droplet and air mixing, which is coupled to evaporation and combustion processes. Past experimental studies [1–5] have identified various jet breakup mechanisms. In regard to the jet breakup length, Kitamura and Takahashi [2] showed that an increase in the cross-flow velocity led to a decrease in the intact length of the jet, to the point of major fracture. In other words, a decrease in the jet to cross-flow momentum flux ratio caused a decrease in breakup length. An equivalent observation was made by Schetz and Padhye [5] in their study of a liquid jet injected into a high subsonic cross-flow. In combustion applications, the fragments resulting from jet injection into a cross-flow most likely experience cross-flow velocities that are high enough such that the shear mechanism becomes the dominant mode in secondary drop breakup. The study of Ranger and Nicholls [6] which involved droplet shattering in a high speed

* Corresponding author. Tel.: +1 256 824 6194; fax: +1 256 824 6839.
E-mail address: cchen@che.uah.edu (C.P. Chen).

0017-9310/$ - see front matter © 2008 Elsevier Ltd. All rights reserved.
doi:10.1016/j.ijheatmasstransfer.2007.11.054

Nomenclature

C_D	drag coefficient	t	time (s)
D_p	droplet diameter	U_r	relative velocity
D_0	initial droplet diameter	We	Weber number
D_{Noz}	injector nozzle diameter	ρ_l	drop liquid phase density (kg/m^3)
h_0	penetration height on the experimental center plane where measured liquid volume flux is 0.01 cc/s cm^2	ρ_g	gas phase density (kg/m^3)
		σ	liquid fuel surface tension coefficient (N/m)
M	Mach number	μ_l	droplet liquid viscosity (kg/m s)
Oh	Ohnesorge number	γ	ratio of specific heats
q_0	jet-to-air momentum flux ratio		
Re	Reynolds number	*Subscripts*	
T_g	gas temperature of environment (K)	g	gas phase property
T_d	bulk temperature of droplet (K)	l	liquid phase property
T_s	surface temperature of droplet (K)	s	droplet surface property

convective air stream at supersonic speeds supports this view. Their study found that the main mode of droplet disintegration was attributed to the stripping of the boundary layer by the shear forces produced by the convective air stream.

For a liquid jet in a supersonic cross-flow, a bow shock occurs due to the disturbance to the incident flow by the transverse injection. The shock strength varies with respect to the distance measured from the injector wall. Away from the wall, the bow shock curves around the injectant plume. Due to the expansion of injected jet and its interaction with the bow shock, complex shock waves are generated in the injectant plume, including a barrel shock and a Mach disk. Due to the blockage to the supersonic cross-flow by the fuel injection, a horseshoe vortex tube is formed near the wall. In the injectant plume a pair of the counter-rotating vortex tubes also develops. Due to the strong aero-thermal–dynamical interaction, the liquid droplets near the liquid/gas interface would heat up while the core region may remain cold (even in cold cross-flow configurations). The heat transfer through conduction and convection (possibly by internal turbulence and circulation) to its interior proceeds until the end of its lifetime. Thus, the droplet evaporation process should be considered in high speed liquid–gas flows.

The complexity of the phenomena outlined above is numerically challenging and computationally intensive. A few recent numerical studies are mentioned here. The atomization modeling study of Im et al. [7] was based on a modified Kelvin–Helmholtz/Rayleigh–Taylor hybrid model and the Eulerian–Lagrangian (E–L) numerical procedure. Droplet evaporation process was not considered in their high speed flow simulation. Using the E–L procedure, an improved boundary layer stripping model coupled with the Rayleigh–Taylor model was developed by Khosla and Crocker [8] for liquid jets in low speed cross-flow. A new methodology combining the jet embedding (JE) technique with the volume-of-fluid (VOF) technique was used by Ryan [9] for liquid jet in low speed air cross-flow simulation. These studies did not include spray evaporation models in their simulations of cold-flow configurations. From the above discussion, expecting droplet evaporation may play a significant role in high speed cross-flow configuration, a newly developed finite-conductivity droplet evaporation model [10] was included in the present study. During the course of study, it was also found out that the drag coefficient correlation used in E–L methodology had a significant effect on droplet dispersion in high speed flow regimes. Thus, the objectives of this study are two fold: the first one is to justify the inclusion of droplet evaporation model and assess the finite-conductivity model [10] in high speed cross-flow configuration. The second objective is to appraise a newly proposed correlation for liquid drop drag coefficient in high speed gas flows by Ortiz et al. [11]. In this paper, validation results will be presented in comparison to the experimental measurements of Lin et al. [3], with a long term-goal of developing numerical capabilities for high speed spray combustion applications including liquid turbulence effects.

2. Numerical modeling approaches

2.1. T-blob and T-TAB atomization/evaporating spray models

The current atomization/spray model is developed for computational analysis based on the Eulerian–Lagrangian numerical approach. Liquid phase is tracked from the injector plane, and the primary atomization, as well as the subsequent secondary breakup is modeled using the T-blob/T-TAB hybrid model [12]. Both primary and secondary droplet breakup processes are modeled and the transition from primary to secondary breakup is modeled based on energy balance. The current atomization/spray model was based on the Kelvin–Helmholtz/Rayleigh–Taylor formulation; however, turbulence within the liquid jet/

spray is accounted by the two-equation k–ε turbulence model formulation. The characteristic turbulent velocity and length scales at the injector exit were modeled through injector characteristics. Detailed model description and validations can be found in Refs. [12,13], and it is suffice to say that within each numerical blob and droplet, turbulence characteristics such as fluctuating velocity level, length and time scales are supplied by the model. It should also be noted that the T-blob/T-TAB model is a sub-grid phenomenological model for primary/secondary droplet breakup using conventional Eulerian–Lagrangian approach [13]. Thus detailed breakup regimes such as column breakup, bag breakup, multi-mode breakup, shear breakup, catastrophic breakup, etc. were not separately modeled. The numerical "blobs" (in primary breakup) and droplets (in secondary breakup) were all assumed to be spherical.

For blob and droplet evaporation, a "two-temperature model" was formulated to account for the finite-conductivity (F-C) effect within the liquid phase. In the two-temperature model, the core (or bulk) temperature (T_d), is assumed well-mixed by convection/turbulence transport. Heat resistance exists at the liquid-side boundary layer region, and the droplet surface temperature (T_s) differs from the droplet core temperature. The heat transfer coefficient across this thin film (or boundary layer) is then formulated through the turbulence characteristics supplied from the T-blob/T-TAB model, to account for the finite-conductivity effect. The boundary layer thickness (or film thickness) was estimated from a turbulent thermal diffusivity based on the T-blob/T-TAB model. Again, detailed model development and validation were described in [10] and is not repeated here.

It should be noted that the current atomization evaporating spray model, although originally developed for low speed gas–liquid flows, was applied to the liquid jet atomization in high speed supersonic cross-flow simulation in this study without modifying the original model. The only exception is the drag coefficient correlation used for droplet velocity and acceleration calculation. This correlation is described in the following section.

2.2. High speed drag coefficient

During the course of this research, the need for updating the existing models in the CFD code for computing the drag coefficient in supersonic flow situations was studied. The existing correlation for estimation of drag coefficient in the CFD ACE+ code [14,15] for compressible flows was based on the model developed by Henderson [16]. To improve upon the accuracy of prediction of the drag coefficient, based on a review of current literature in this area of research, focus was made on the model developed by Ortiz et al. [11] for liquid droplets exposed to a high speed air stream. In drop breakup studies, the most widely used dimensionless parameters are the Weber number and the Ohnesorge number. For free stream Mach number in the range 0.7–1.7, Ortiz et al. proposed an empirical bi-power formula for the drag coefficient:

$$C_D = 1.6 + 0.4Oh^{0.8}We^{0.01}, \tag{1}$$

where We is the Weber number given by

$$We = \left(\frac{\rho_g U_r^2 D_p}{2\sigma}\right) \tag{2}$$

and Oh is the Ohnesorge number given by

$$Oh = \frac{\mu_l}{\sqrt{\rho_l \sigma D_p}}. \tag{3}$$

Extensive experimental data was compiled and used in [11] to establish the correlation shown in Eq. (1). Newtonian liquids covering a range of viscosities from 0.001 to 10 kg/m s. and shock Mach numbers ranging from 2.0 to 4.7 were studied to arrive at the correlation. Based on the preliminary two-way coupled results during the course of this research this model was incorporated into the CFD code to evaluate its numerical effectiveness. For comparison, the classical low speed drag coefficient correlation and the model of Henderson [16] are described here. The low speed classical incompressible flow drag coefficient is given by the standard drag curve [17], where

$$\begin{aligned} C_D &= \frac{24}{Re}\left[1 + \frac{Re^{2/3}}{6}\right] \quad \text{for } 1 < Re < 10^3, \\ C_D &= 0.44 \quad \text{for } Re > 10^3. \end{aligned} \tag{4}$$

Henderson's [16] correlation to calculate the drag coefficient consists of one equation for the subsonic region given by Eq. (5) and one for the supersonic region given by Eq. (6). Depending on the local relative Mach number the appropriate correlation is used.

Subsonic regime:

$$\begin{aligned} C_{D_{sub}} = {} & \frac{24}{Re + S_r\left\{4.33 + \frac{3.65 - 1.53T_r e^{\left(-0.247\frac{Re}{S_r}\right)}}{1 + 0.353T_r}\right\}} \\ & + \left\{\frac{4.5 + 0.38\left[0.03Re + 0.48\sqrt{Re}\right]}{1 + 0.03Re + 0.48\sqrt{Re}} + 0.1M^2 + 0.2M^8\right\} \\ & \times e^{\left(-\frac{M}{2\sqrt{Re}}\right)} + 0.6S_r\left(1 - e^{\frac{M}{Re}}\right). \end{aligned} \tag{5}$$

Supersonic regime:

$$C_{D_{sup}} = \frac{0.9 + 1.86\sqrt{M/Re}\left(2 + \frac{2}{S_r^2} + \frac{1.058\sqrt{T_r}}{S_r} - \frac{1}{S_r^4}\right)}{1 + 1.86\sqrt{M/Re}}, \tag{6}$$

where $T_r = \frac{T_d}{T_g}$ and the molecular speed ratio, $S_r = M\sqrt{\gamma/2}$.

3. Validation results and discussion

The current models were implemented into an existing CFD code, CFD ACE+ [15] for two-way coupling Euleri-

an–Lagrangian calculations. In this paper the numerical results to simulate the experimental 3D liquid jet in supersonic cross-flow cases [3] are presented. Again, Ref. [14] should be consulted for detailed numerical (such as grids and time steps) implementation issues.

Fig. 1 shows the three-dimensional computational domain with dimensions of $762 \times 152 \times 127$ mm, discretized with an initial grid distribution $130 \times 40 \times 40$. Refined grids used for the preliminary numerical computations around the liquid injection region were also shown. The inlet boundary conditions for the chamber were given by a static pressure of 29 kPa, a static temperature of 304.1 K and a flow velocity of 679 m/s based on a free stream Mach number of 1.94. The injection velocity of the spray jet was determined based on a jet-to-air momentum ratio $q_0 = 7.0$. In this study the water jet injection temperature was set to 300 K. The injection nozzle diameter (D_{Noz}) was 0.5 mm and located at a distance of 139 mm from the chamber inlet. A computational time step of 2.5×10^{-6} s was used with an injection period of 4 μs. Comparison of liquid jet penetration heights computed using the classical infinite-conductivity (I-C) model and the finite-conductivity model (F-C), and the correlated experimental measurement is shown in Fig. 2. The classical low speed drag coefficient correlation (Eq. (4)) was used for this simulation. To be consistent with the PDPA measurement, the spray penetration height is defined as the location where the calculated liquid volume flux to be 0.01 cc/s cm^2 at the $Z = 0$ center plane. The experimental correlation for the penetration height (h_0/D_{Noz}) is given by [3], $h_0/D_{\mathrm{Noz}} = 4.73 q_0^{0.3} (X/D_{\mathrm{Noz}})^{0.3}$, where X is the axial location referenced from the jet inlet and D_{Noz} the injector orifice diameter. Based on the initial results for tip penetration (Fig. 2), computed with the T-blob/T-TAB model and the associated low speed droplet drag law without adjusting any model constants it was concluded that the jet penetration increased rapidly in the vicinity of the injector exit and then gradually increased due to the increase in the velocity of the air stream. The momentum of the spray droplets also increases in the direction of the supersonic

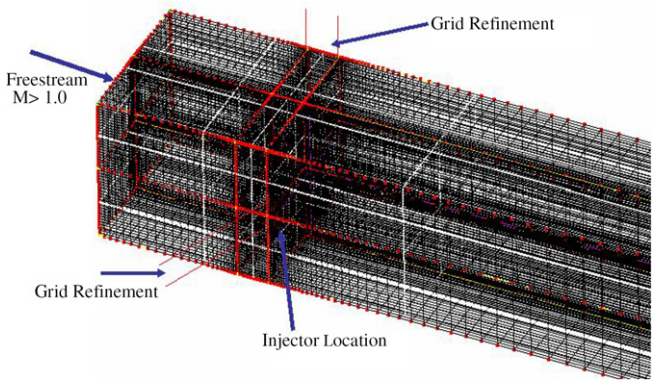

Fig. 1. Three-dimensional computational domain and mesh of the liquid jet in cross-flow.

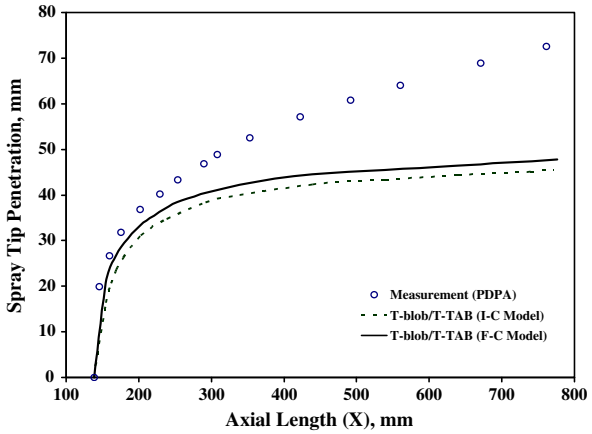

Fig. 2. Comparative Spray tip penetrations for I-C and F-C models with measurements.

airflow due to acceleration by the airflow. The droplets have been observed to accelerate to supersonic speeds in a later part of the spray. Inamura et al. [18] indicated that the acceleration of the droplets results in lower relative velocities, thereby lowering the drag force of the air stream. Further improvement in drag law to account for the high speed effect was found to be necessary to account for supersonic acceleration of the droplets.

To improve the numerical prediction of supersonic drag coefficient, the empirical correlation of Eq. (1) was incorporated into the CFD code and the same test case was simulated. The focus of this test was to evaluate the improvement in spray tip penetration for the F-C model with the prediction, using different drag coefficient correlations. The results of the computations are shown in Fig. 3. The results from Fig. 3 indicate a significant improvement in the prediction of the tip penetration length, both in the near injection region and the downstream region of the injection region using the correlation of Ortiz et al. [11].

The above numerical results indicate the improvements of the C_{D} model in predicting the spray tip penetration,

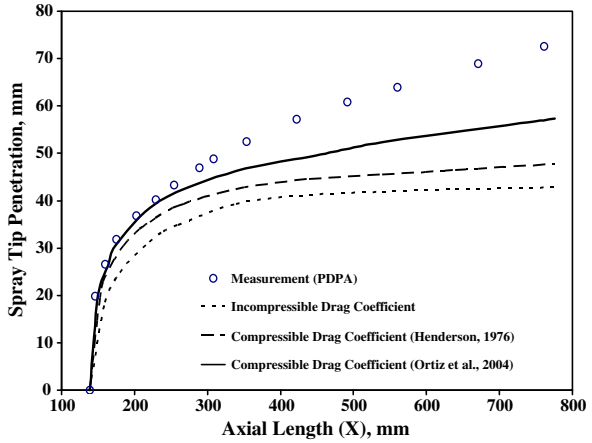

Fig. 3. Improvement of spray tip penetration of F-C model with drag coefficient modification.

specifically at the region near the jet injection location. The supersonic flow interacts with the liquid fuel jet near the injection location causing a rise in gas flow temperature. The result of this interaction causes the liquid fuel droplets to heat up. The improvements of the finite-conductivity (F-C) evaporation model in predicting the tip penetration at the near injection region is due to the fact that the droplet bulk temperature (T_d) is lower than that predicted using the infinite-conductivity (I-C) model as shown in Fig. 4a and b. In the I-C model, the droplet core temperature is higher than that of the F-C model. In two-way coupled droplet evaporation simulation, this lead to faster evaporation and resulted in smaller drop sizes in the near injector region. On the other hand, the F-C model predicts larger drop sizes than the I-C model does. Subsequently a longer tip penetration length is predicted by the F-C model. The momentum of the spray droplets also increases in the direction of the supersonic airflow due to acceleration by the airflow.

The prediction of droplet velocity (U_d) and the Sauter mean diameter (SMD) along the Y-direction, at measurement location $X = 50$ mm are shown in Fig. 5a and b, respectively. The flux-average properties (as described in

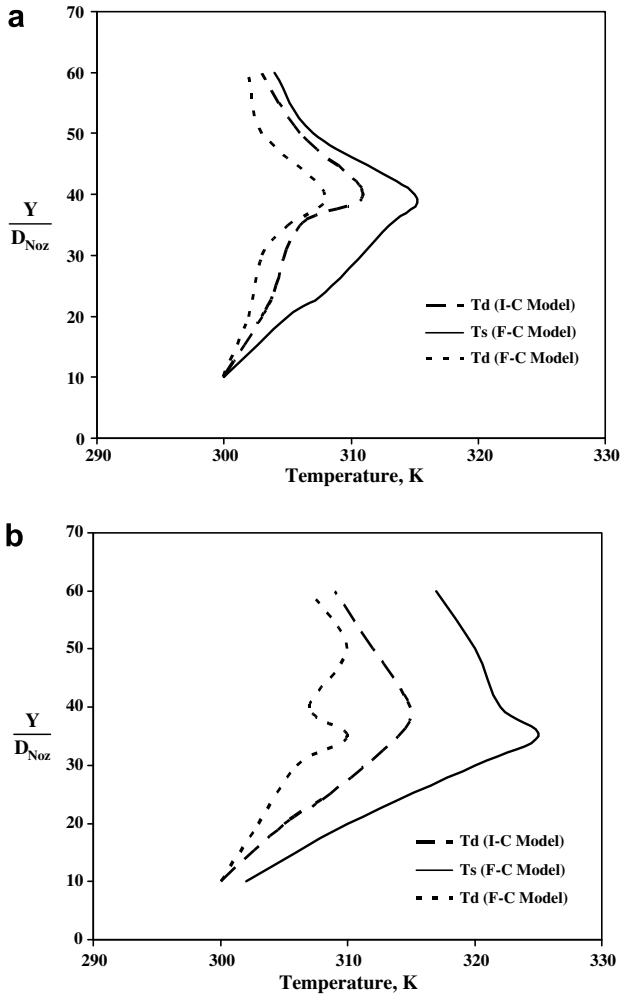

Fig. 4. Droplet temperature profiles for I-C and F-C models at: (a) $X = 30D_{Noz}$ and (b) $X = 50D_{Noz}$.

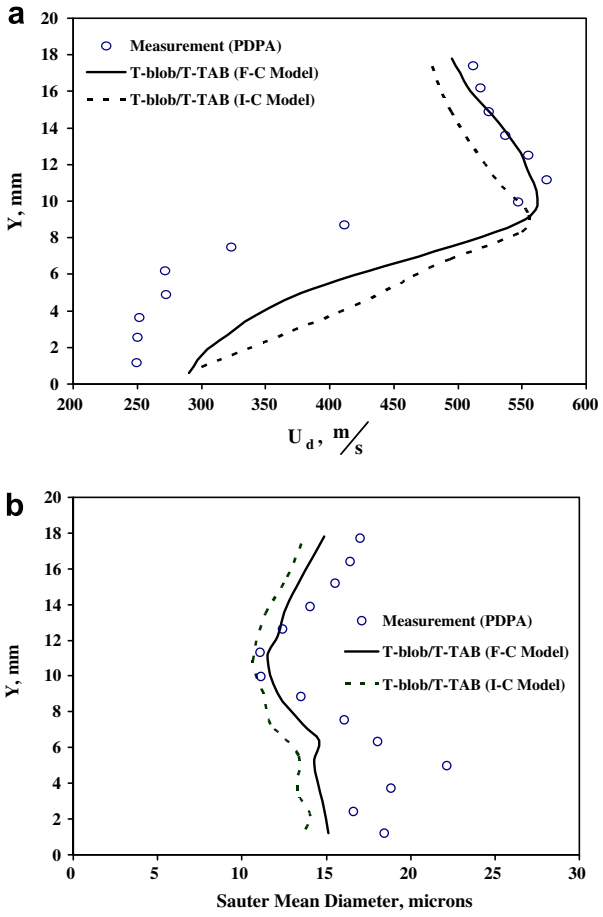

Fig. 5. (a) Comparisons of averaged droplet axial velocity profiles at $X = 50$ mm and (b) comparisons of SMD profiles at $X = 50$ mm.

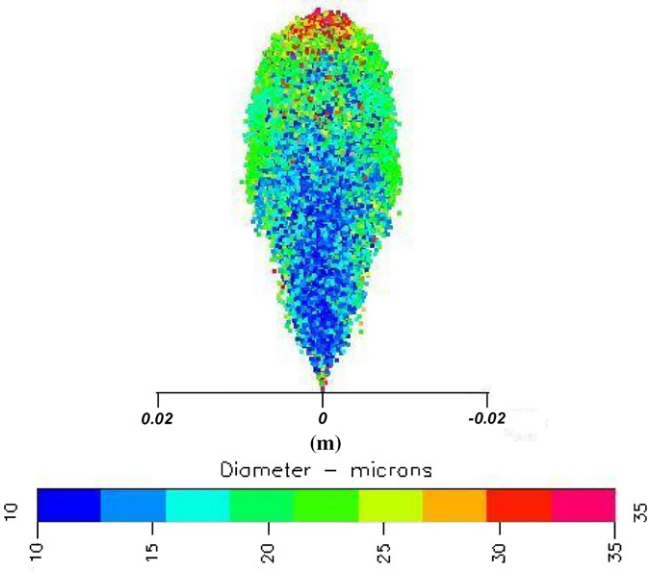

Fig. 6. Liquid jet structures and droplet size distributions (back-view) near injection point.

[13]) were used. The numerical results of the droplet velocity profiles (Fig. 5a) appear to have different trends in the initial bulk region of the spray core in comparison with measured data. However, the trend in the Y-direction is in reasonable agreement with the measurement. The SMD profiles along the Y direction at $X = 50$ mm (Fig. 5b) shows a reasonable trend in comparison with measured data further away from the bottom wall of the combustor. In comparison between the I-C and F-C models, the velocity and drop size distributions predicted from the F-C model have a closer agreement with the test data. It should be pointed out that inlet liquid jet turbulence is sensitive to spray dynamics as indicated by the recent experiments conducted by Mayinger and Gruenig [19]. The inlet liquid jet turbulence levels used in this simulation study were estimated by the method described in [10]. Considering the uncertainties associated with the jet inlet conditions, the numerical results show reasonable agreement with experimental data.

The high velocity droplets are mainly distributed at the top of the spray plume in a kidney or horseshoe shape. It is observed from the SMD distribution in the spray plume that the larger droplets are distributed at the outer periphery of the spray core, in a horseshoe shaped manner. The inner core of the spray plume consisted of smaller size droplets. The larger droplets possess higher momentum compared to the smaller sized droplets. Fig. 6 shows the back-view of the spray plume near the injection point to illustrate the droplet size distributions.

The solution sensitivity to grid refinement in the near injection region was also studied. A refined grid discretized by $145 \times 50 \times 40$ in the X, Y and Z directions, clustered to $X = 100D_{\mathrm{Noz}}$ in the X direction and between $Y = 20D_{\mathrm{Noz}}$ and $Y = 80D_{\mathrm{Noz}}$ in the Y direction, was used for this study and computations performed using the compressible drag correlation of Ortiz et al. [11], with the F-C model. Fig. 7 shows a marginal improvement in the tip penetration prediction at the near injection region, but further downstream the results do not differ significantly from the coarse grid computations, indicating the grid independency of the numerical computations in the near injector region. Further computational studies are required to study effects of grid resolution in the downstream region of the combustor. The difference in the spray tip penetration in the downstream region could also

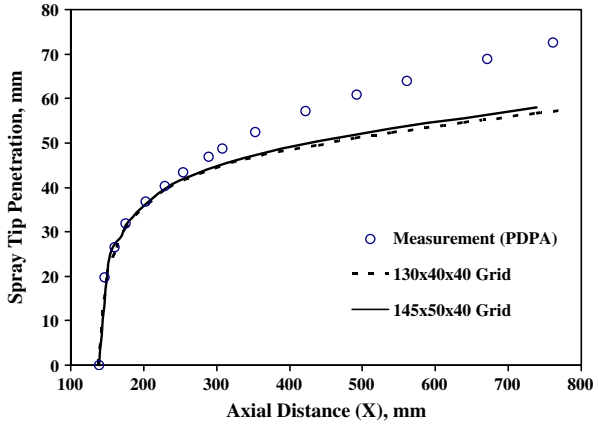

Fig. 7. Effect of grid refinement on spray tip penetration prediction.

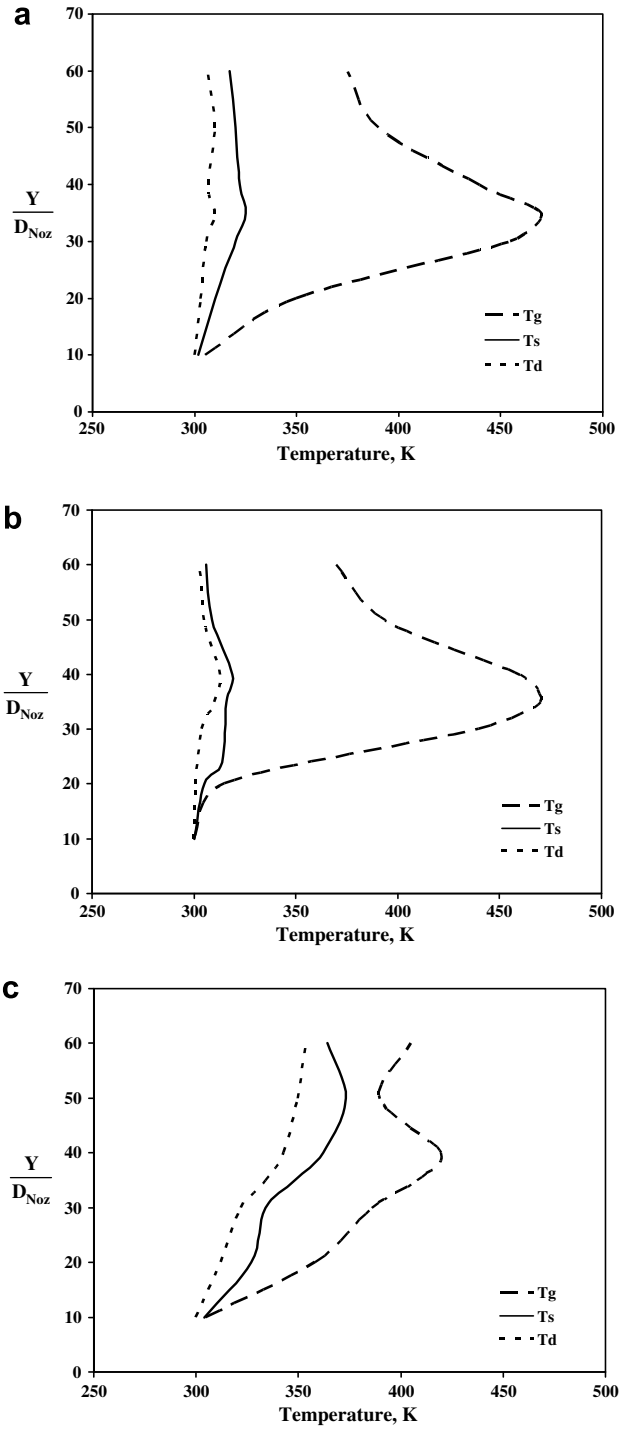

Fig. 8. Droplet and gaseous stream temperature profiles along normalized Y at (a) $X = 30D_{\mathrm{Noz}}$, (b) $X = 50D_{\mathrm{Noz}}$, and (c) $X = 700D_{\mathrm{Noz}}$.

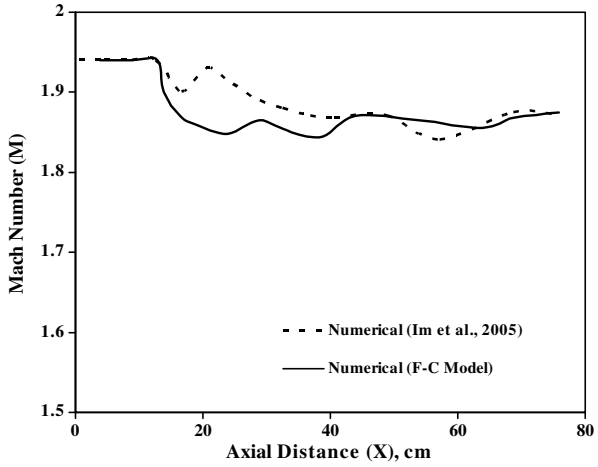

Fig. 9. Center-line ($Z = 0$ plane) Mach number profile along the outer periphery of the spray plume in the axial (X) direction.

be attributed to the manner in which the rate of mass reduction of the parent droplet is computed in the T-blob/T-TAB atomization models. In the turbulent atomization models, the liquid mass reduction or mass shed from the parent parcel is tracked during the computation. In the numerical model of Trinh and Chen [12,13] a new parcel was produced from the jet surface when the mass shed from the droplet (parcel) reaches or exceeds 3% of the injected parcel mass and the number of generated drops was greater than the number of parent drops. This mass reduction practice was used in this study without further adjustment. The improved drag coefficient has no direct relation with the rate of mass reduction used in this study. This rate of mass reduction is a key mechanism in numerical spray computations. The current methodology in determining the mass-loss can be modified to improve accuracy of predictions in the downstream region. In the numerical study of [7], a modified mass-loss formulation was proposed to couple with the Kelvin–Helmholtz/Rayleigh–Taylor atomization/spray model in order to match the penetration envelop data of [3].

The variation of the free stream gas temperature (T_g) with that of the drop surface temperature (T_s) and the drop bulk temperature (T_d) at three different axial locations in the normalized Y direction are shown in Fig. 8a–c. From Fig. 8a it can be observed that the free stream gas temperature rises to a high value (≈480 K) in the immediate vicinity of the barrel shock region at $X = 30D_{Noz}$. The drop surface temperature reaches a maximum of about 325 K, indicating that the relative velocity between the droplet and the free stream is high (a high C_D) and therefore a high level of internal turbulence within the droplet. The droplet core temperature at the maximum surface temperature is about 307 K. Further downstream at $X = 50D_{Noz}$, as seen from Fig. 8b, the free stream gas temperature still remains high and the maximum drop surface temperature increases slightly to about 335 K and the maximum core temperature to about 308 K. The difference in the drop surface temperature and the core temperature, in Fig. 8a and b shows that the boundary layer thickness increases with the surface of the drop heating up quicker than droplet core. Further downstream at $X = 700D_{Noz}$, in Fig. 8c, the free stream gas temperature decreases (≈420 K) as the droplets heat up and exchange heat and mass with the free stream. The maximum droplet surface temperature rises to about 355 K while the maximum drop bulk temperature rises to about 348 K. The velocity of the droplets increases at this point to match the free stream velocity, the relative velocity decreases and consequently the turbulence within the liquid droplet decreases.

The temperature profiles represented by Fig. 8a–c provide a more realistic representation of the evolution of the droplet thermal boundary layer thickness where the boundary layer thickness is initially thick and gradually becomes thinner with respect to the droplet internal turbulence. These temperature profiles also indicate the necessity of using droplet evaporation model in such high speed test case [3]. The inclusion of droplet evaporation effect may explain the drastically different spray dynamics results from [7], even the gas phase cross-flow dynamics were similar. Fig. 9 shows the center-line ($Z = 0$) gas stream Mach number profile in comparison to the numerical computations of Im et al. [7] along the X–Y plane on the periphery of the spray plume.

The gas stream temperature contours along the normalized axial direction at different Y plane locations are shown in Fig. 10. Fig. 10a–c shows the temperature contours at $X = 20D_{Noz}$, $30D_{Noz}$ and $50D_{Noz}$, respectively, in the Y–Z plane. It can be observed that the free stream (gas) temperature is high in the region of high relative velocity. The fuel vapor mass fraction contours are shown in Fig. 11a–c at $X = 20D_{Noz}$, $30D_{Noz}$ and $50D_{Noz}$ respectively, along the Y–Z plane. From Fig. 11a, it could be observed that the evaporation rate is high in the core region of the spray plume with smaller size droplets. Near the injector exit, the two-phase slip velocity is highest and encounters the low pressure, high temperature region near the Mach disk. Further downstream as seen from Fig. 11b and c, the mass transfer region within the spray plume from the droplet surface to the free stream increases from the core to the periphery in concert with the temperature contours shown previously.

4. Concluding remarks

We have applied a newly developed finite-conductivity model for evaporating spray numerical calculations of a liquid jet atomization/spray in high speed cross-flows. In this two-way Eulerian–Lagrangian multi-dimensional full CFD simulation, the current finite-conductivity model coupled with the T-blob/T-TAB model show superior performance to conventional infinite-conductivity evaporation models when comparing with the experimental data.

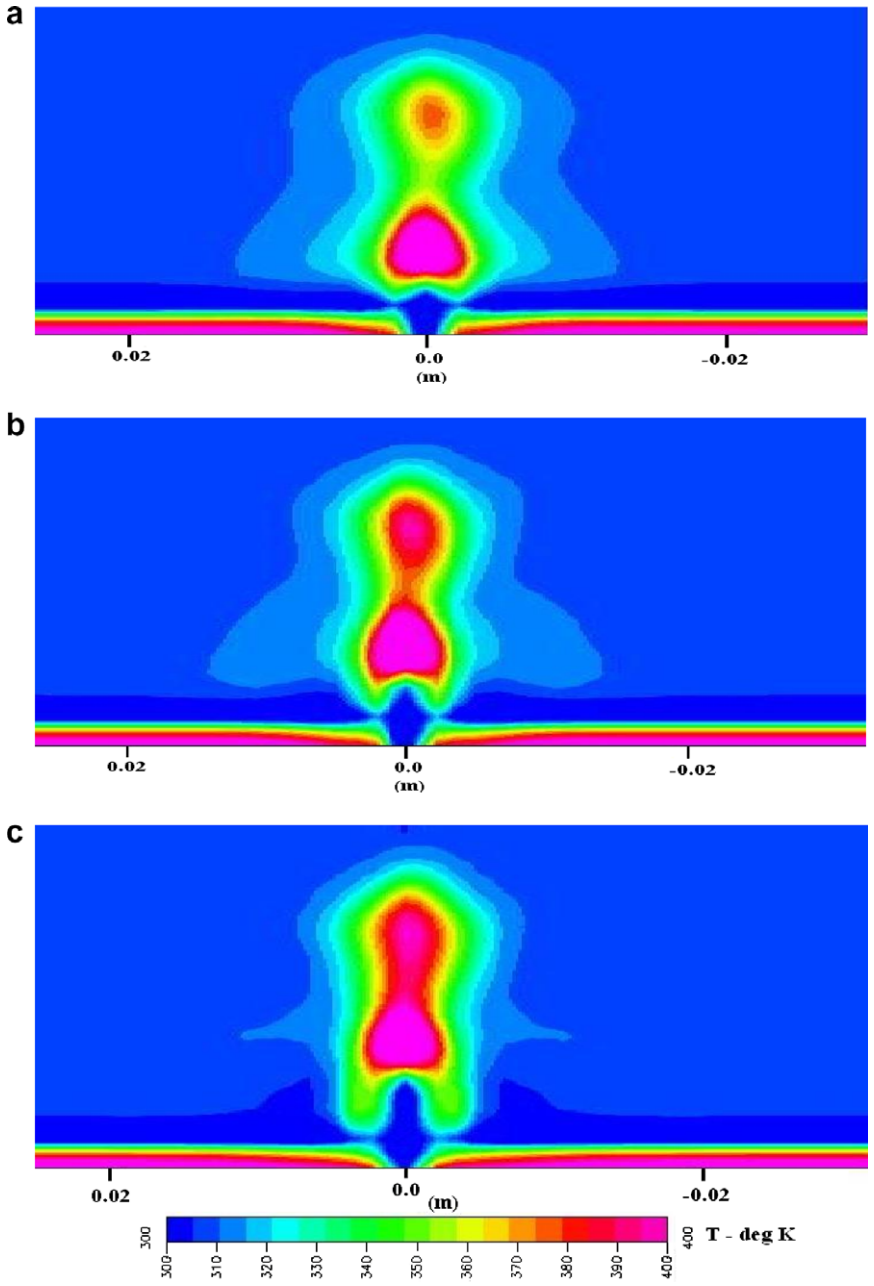

Fig. 10. Y–Z plane temperature (T_g) contours at (a) $X = 20D_{Noz}$, (b) $X = 30D_{Noz}$ and (c) $X = 50D_{Noz}$.

The numerical results also indicate the need of including droplet evaporation mechanisms even for cold-flow configurations due to strong aero-thermal interaction between the supersonic cross-flow and the liquid jet. The incorporation of a recently developed empirical high speed droplet drag laws [11] indicated further improvement in the prediction of the tip penetration length, both in the near injection region and the downstream region of the injection region. The droplet velocity and size (SMD) computations, using the F-C model, were found to be closer to the measured data in comparison to the computations with the I-C model. The grid sensitivity study results indicated small improvement in the prediction at the near injection region, but further downstream the results of the refined grid computations did not differ significantly from the coarse grid computations, indicating a grid independent solution in the near injector region. The modeling of mass reduction rate from the droplet (parcel) in T-blob/T-TAB atomization/spray model was found to have critical effects on the spray distribution. Future work should focus towards incorporating more fundamental numerical approaches, such as coupled volume of fluids (VOF)/direct numerical simulations (DNS) approach of resolving near field liquid column dynamics, to obtain more accurate descriptions of the physical mass reduction phenomenon.

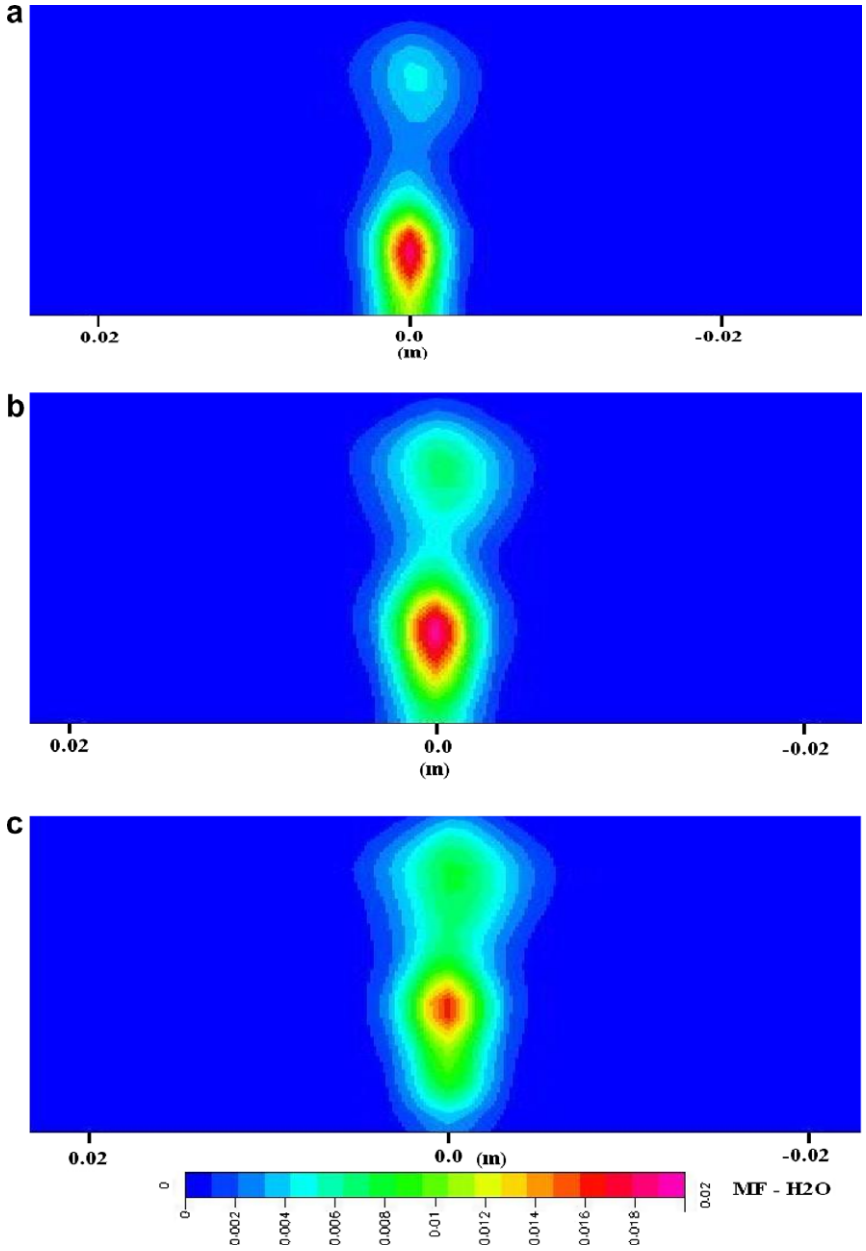

Fig. 11. Y–Z plane fuel mass fraction contours at (a) $X = 20D_{Noz}$, (b) $X = 30D_{Noz}$ and (c) $X = 50D_{Noz}$.

Acknowledgements

This study was partially supported by NASA Grant NCC8-200 through the UAH Propulsion Research Center. The authors would also like to acknowledge the use of the CFD ACE+ code under an educational agreement with CFD Research Corporation.

References

[1] T.H. Chen, C.R. Smith, D.G. Schommer, A.S. Nejad, Multi-zone behavior of transverse liquid jet in high-speed flow, AIAA-paper 93-0453, 1993.
[2] Y. Kitamura, T. Takahashi, Stability of a liquid jet in air flow normal to the jet axis, J. Chem. Eng. Jpn. 9 (4) (1996) 282–286.
[3] K.C. Lin, P.J. Kennedy, T.A. Jackson, Structures of water jets in a Mach 1.94 supersonic crossflow, AIAA-paper 2004-0971, 2004.
[4] M. Pilch, C.A. Erdman, Use of breakup time data and velocity history data to predict the maximum size of the stable fragments for acceleration-induced breakup of a liquid drop, Int. J. Multiphase Flow (13) (1987) 741–757.
[5] J.A. Schetz, A. Padhye, Penetration and breakup of liquids in subsonic airstreams, AIAA J. 15 (10) (1977) 1385–1390.
[6] A.A. Ranger, J.A. Nichols, Aerodynamic shattering of liquid drops, AIAA J. 7 (2) (1969) 285–290.
[7] K.S. Im, K.C. Lin, M.C. Lai, Spray atomization model of liquid jet in supersonic cross flows, AIAA-paper 2005-0732, 2005.
[8] S. Khosla, D.S. Crocker, A boundary layer stripping CFD model for shear regime atomization of plain liquid jets in cross flow, ILASS Americas, in: 17th Conference on Liquid Atomization and Spray Systems, Arlington, VA, May 2004.

[9] M. Ryan, CFD prediction of the trajectory of a liquid jet in a non-uniform air crossflow, Comput. Fluids 35 (2006) 463–476.
[10] M.S. Balasubramanyam, C.P. Chen, H.P. Trinh, A new two-temperature model for evaporating atomization and spray, J. Heat Transfer 129 (8) (2007) 1082–1086.
[11] C. Ortiz, D.D. Joseph, G.S. Beavers, Acceleration of a liquid drop suddenly exposed to high-speed air-stream, Int. J. Multiphase Flow 30 (2004) 217–224.
[12] H.P. Trinh, C.P. Chen, Modeling of turbulence effects on liquid jet atomization and breakup, Atomization Spray. 16 (2006) 907–932.
[13] H.P. Trinh, C.P. Chen, M.S. Balasubramanyam, Numerical simulation of liquid jet atomization including turbulence effects, J. Eng. Gas Turb. Power 129 (4) (2007) 920–928.
[14] M.S. Balasubramanyam, Modeling turbulence effects on the heat and mass transfer of evaporating sprays, Ph.D. Dissertation, Department of Mechanical and Aerospace Eng., University of Alabama in Huntsville, 2006.
[15] CFD Research Corporation, ACE+ Theory Manual, 2004.
[16] C.B. Henderson, Drag coefficients of spheres in continuum and rarefied flows, AIAA J. 14 (6) (1976) 707–708.
[17] G.B. Wallis, One-dimensional two-phase flow, second ed., McGraw-Hill, New York, 1969.
[18] T. Inamura, M. Takahashi, A. Kimakawa, Combustion characteristics of a liquid fueled Ramjet combustor, J. Propul. Power 17 (4) (2001) 860–868.
[19] F. Mayinger, C. Gruenig, Supersonic Combustion of kerosene/H_2 mixtures in a model Scramjet combustor, Inst. for Thermodynamics, Munich, Germany, 2005.